NANO LETTERS

pubs.acs.org/NanoLett Letter

Controlled Fabrication of DNA Molecular Templates for *In Situ* Formation and Measurement of Ultrathin Metal Nanostructures

Jorge L. Barreda, Longqian Hu, Liuqi Yu, Jacob Hudis, Timothy D. Keiper, Junfei Xia, Zhibin Wang, Jingjiao Guan, and Peng Xiong*

Cite This: *Nano Lett.* 2020, 20, 8135–8140 Read Online

ACCESS | Metrics & More | Article Recommendations | Supporting Information

ABSTRACT: Fabrication of ultrathin metal nanostructures usually requires some combination of high-vacuum deposition and postgrowth processing, which precludes access to nanostructures of ultrasmall cross sections for most materials. DNA nanowires (NWs) are versatile insulating templates with intrinsic sub-10 nm line width. Here, we demonstrate a method of DNA template fabrication with precise control over the location and orientation of the DNA NWs. We further demonstrate that this template can be used to support formation of ultrathin metal NWs for derivative nanodevices: a metal is incrementally deposited, and electrical transport measurement is performed *in situ* at each step. The results show a homogeneous metal NW is obtained at a thickness as small as 0.9 nm with a cross-section of only a few nm^2. The high degree of control in the location, separation, and orientation of the DNA NWs affords this method great promise in fabricating complex nanodevices based on metal NWs.

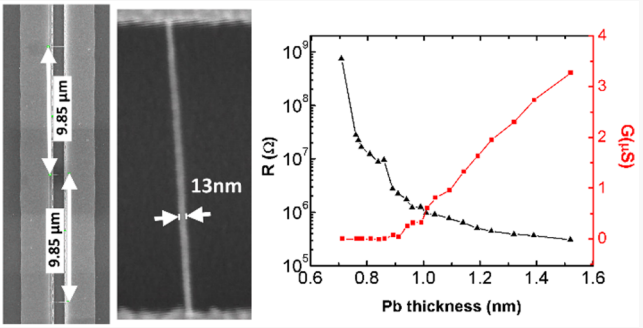

KEYWORDS: *Metal nanowires, ultrathin nanostructures, DNA nanowires, molecular template*

Nanowires (NWs) are an essential class of nanomaterials for the studies of emergent quantum physics due to dimensional confinement and as the basis for a variety of nanotechnology applications,[1,2] including microelectronics,[3,4] photonics,[5] chemical and biomolecular sensing,[6−8] and more recently, topological quantum computation.[9−12] There have been significant advances in the synthesis and integration of NWs in both the top-down and bottom-up approaches;[13,14] however, challenges remain in both schemes for realizing the smallest possible NWs and most precise placement in device structures. This is especially so for ultrathin metal NWs susceptible to oxidation and other chemical reactions in ambient air. Various types of semiconductor NWs have been mass-produced by vapor and solution synthesis, and the resulting NWs are generally stable in ambient air after the formation of a thin native oxide layer; in contrast, similar successes in fabricating ultrathin metal NWs have been limited to a handful of noble metals. The more common methods of fabricating ultrathin metal nanostructures involve some combination of (ultra)high-vacuum thin film deposition and pre- and/or postgrowth lithography and processing. The unavoidable ambient exposure in the process makes it extremely difficult, if not impossible, to obtain nanostructures at single or a few monolayer thicknesses for most metals.

One method that could circumvent this problem utilizes molecular templates on which metal can be deposited and metal nanostructures can be formed directly without any post growth processing. Over the years, both DNA wires and insulating carbon nanotubes[15−18] have been used as templates for the fabrication of ultrathin metal NWs; however, in all cases the DNA wires or carbon nanotubes were randomly assembled without control over the number, orientation, and location of the NWs. Here, we report a process of producing NWs of sub-10 nm widths and down to monolayer thicknesses with precise placement. The method is widely applicable to a broad variety of metallic materials and different growth techniques. The method relies on templates of suspended DNA wires as the substrate. The DNA wires are first formed across an array of micropillars of deliberately designed size and spacing on a polydimethylsiloxane (PDMS) stamp using a one-step dewetting and stretching of DNA molecules.[19,20] The DNA NWs are then transferred from the stamp onto a three-layer substrate ($Si/SiO_2/Si_3N_4$), via microcontact printing, over and across a trench lithographically defined in the intermediate SiO_2 layer with an overhang by the top Si_3N_4 layer.

We further demonstrate that such a template can be used to support the growth of ultrathin, electrically continuous metal

Received: August 1, 2020
Revised: October 4, 2020
Published: October 13, 2020

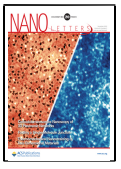

https://dx.doi.org/10.1021/acs.nanolett.0c03166
Nano Lett. 2020, 20, 8135–8140

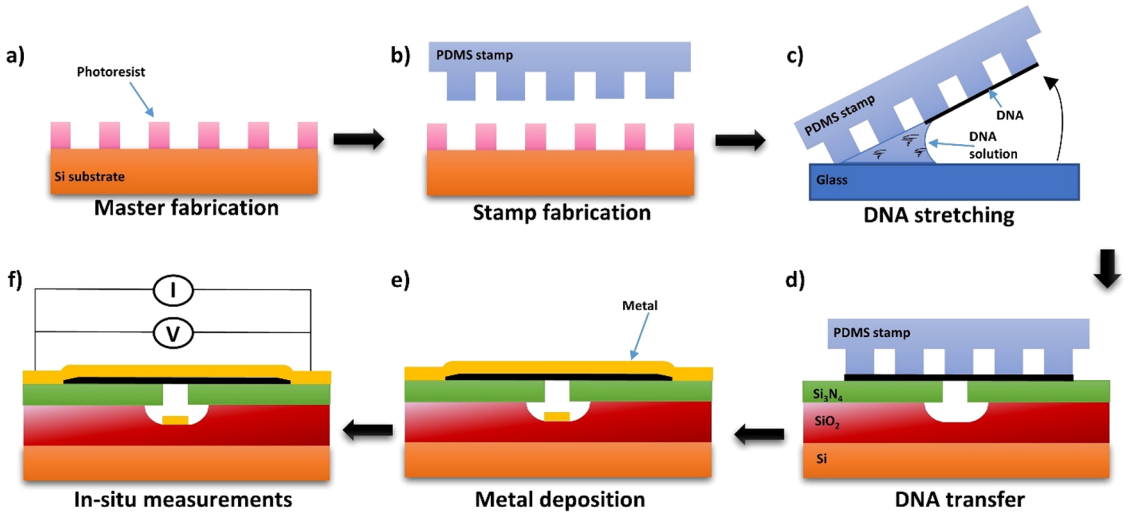

Figure 1. Schematic diagram of the NW fabrication process. (a) Fabrication of the stamp master by photolithography. (b) Formation of the PDMS stamp, which consists of a regular array of micropillars defined by the master. (c) DNA NW stretching on top of the micropillars with the technique described in Experimental Methods in Supporting Information. (d) Transfer of DNA NWs from the stamp to a prefabricated $Si/SiO_2/Si_3N_4$ substrate via microcontact printing. (e) Metal coating of the substrate containing the DNA NW crossing a trench with a Si_3N_4 overhang. (f) *In situ* $I-V$ measurement of the metal NW.

NWs: under high vacuum and at ambient or cryogenic temperatures, a metal is incrementally deposited onto such a template, and electrical transport measurement is performed on individual NWs *in situ* at each step. The results show that by low-temperature quench-condensation on a DNA template, a metal NW of uniform morphology and electrical continuity can be obtained at a thickness of approximately 0.9 nm and widths approaching 10 nm, resulting in a structurally and electrically homogeneous metal NW of cross-section as small as a few nm^2. Our approach for the fabrication of DNA molecular templates is capable of precisely controlling the separation and orientation of the resulting metal NWs.

The entire process of DNA wire fabrication, metal deposition, and electrical measurement is depicted schematically in Figure 1. The process begins with the fabrication of the PDMS stamp, which is utilized to controllably stretch the DNA molecules to form suspended DNA NWs. Stretching of the DNA is based on the procedure developed by Guan et al.[19,20] and briefly described in Experimental Methods in Supporting Information. The procedure results in stretched DNA bundles (NWs) suspended across the pillars on the PDMS stamp, which are then transferred to a prefabricated $Si/SiO_2/Si_3N_4$ substrate. Finally, the suspended DNA template is metalized to form ultrathin metal NWs.

Figure 2a shows an optical image of a PDMS stamp. The inset depicts the three parameters, (a,b,c), that define the geometry of the stamp in μm. This stamp is characterized by (1,7,10); stamps of the same geometry were used for DNA stretching shown in Figure 2b,d. Figure 2b,c shows fluorescent microscopy images of stretched Lambda-DNA labeled with YOYO-1 on top of the micropillars of a PDMS stamp. Figure 2c is a close-up of the image which shows more clearly the suspended DNA NWs across the pillars on a (3,7,3) PDMS stamp. Figure 2d demonstrates that the stretching process is also viable for salmon-DNA fluorescently labeled with rhodamine; in this case, the fluorescence microscopy image shows the DNA wires after being transferred onto a glass slide. Right before the transfer, the substrate is treated in oxygen plasma for 1 min at low power in a tabletop plasma cleaner in

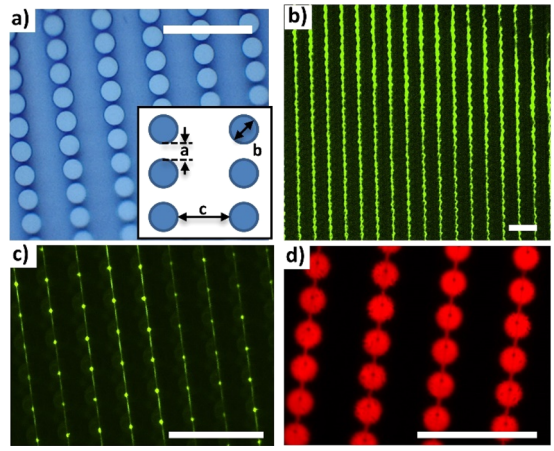

Figure 2. DNA NW fabrication and transfer. (a) An optical image of a PDMS stamp. The inset depicts the three parameters, (a,b,c), that define the geometry of the stamp. (b) A large-area fluorescent microscopy image of a PDMS stamp after the DNA stretching process, showing Lambda-DNA wires labeled with YOYO-1 on top of the micropillars. (c) A close-up fluorescent microscopy image of the Lambda-DNA wires on a PDMS stamp. (d) A fluorescent microscopy image of salmon-DNA fluorescently labeled with rhodamine after being transferred to a glass slide. The scale bars in all panels indicate a length of 30 μm.

order to promote the transfer of the DNA from the stamp to the substrate.

The resulting DNA wires on the PDMS stamp exhibit well-defined orientation and separation. The morphology of such DNA nanowires produced with a similar procedure was characterized in detail by Guan et al.[19,20] Diameters of 3.1 ± 1.1 nm were reported for Lambda-DNA wires.[20] It was found that the DNA wire diameter was correlated with the DNA concentration and the stamp geometry. In general, long and smooth DNA wires could be formed with sub-10 nm diameters. The control in orientation and separation is a unique feature that distinguishes our fabrication scheme from those previously reported[16,17] where the final location and

https://dx.doi.org/10.1021/acs.nanolett.0c03166
Nano Lett. 2020, 20, 8135−8140

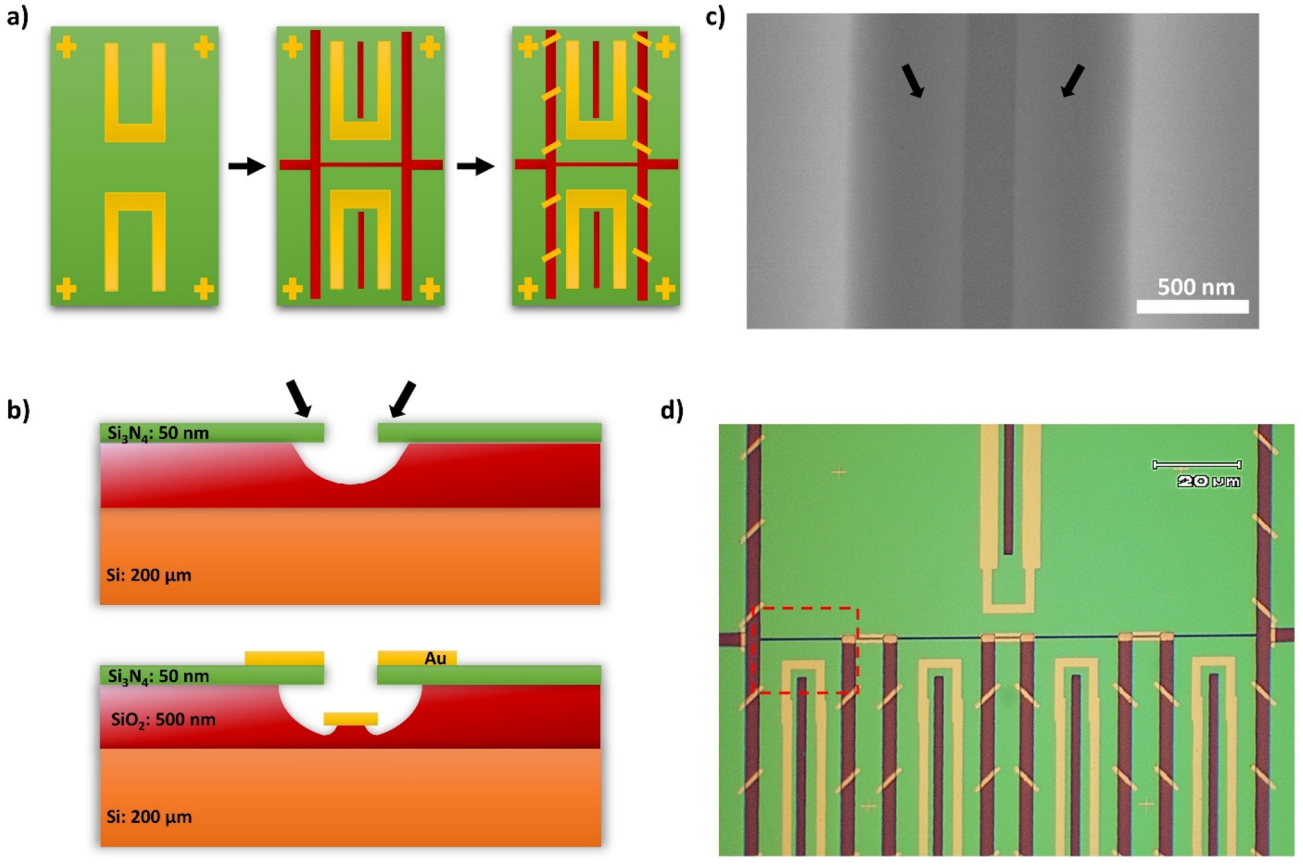

Figure 3. $Si/SiO_2/Si_3N_4$ substrate fabrication for the molecular templates. (a) Schematic diagrams depicting the fabrication process for the substrates, which consists of the definition of alignment marks and Au contacts, the definition of the trenches for electrical isolation, and definition of Au stripes for the electrical isolation inside the trench. (b) Top panel: Schematic diagram of the cross-section of a trench in the substrate after step II in (a). The overhang formed in the Si_3N_4 layer is indicated by the two black arrows. The overhang provides electrical isolation after the metal deposition between the two sides of the trench. Bottom panel: Schematic diagram of the cross-section of a trench in the substrate after step III in (a). The overhang formed under the Au stripes in the trench breaks the conducting path from any broken DNA wire (after the metal coating). (c) A top-view SEM image of a trench formed in the $Si/SiO_2/Si_3N_4$ substrate. The Si_3N_4 overhang is identified by the two black arrows and is clearly visible as the dark regions on both sides of the trench. (d) Optical image of a completed substrate showing one Au electrode on one side of the trench and four electrically isolated Au electrodes on the other side. The substrate can thus accommodate four individual DNA wires; each can support an individual metal NW. The dashed square indicates a region whose close-up view is obtained from SEM and shown in Figure 4.

orientation of the molecular wires were random on the final molecular templates. Precise transfer of the DNA wires with known separation and orientation means we can design and fabricate the substrate to allow independent electrical measurement of multiple individual metal NWs on one and the same device. We illustrate this intriguing possibility using deliberately designed and fabricated $Si/SiO_2/Si_3N_4$ substrates.

Figure 3a shows a schematic flow diagram of the substrate fabrication process. The starting wafer is Si with 500 nm of SiO_2 and 50 nm of low-stress Si_3N_4. Following the fabrication details described in Experimental Methods in Supporting Information, we first define a set of gold alignment marks (Cr/Au, 5/35 nm) via electron-beam lithography (EBL) and thermal evaporation for the subsequent location of the metal electrodes (Cr/Au, 5/50 nm) and trenches. The Au electrodes are designed so that subsequent electrical measurements are in a quasi-four-terminal setup. A set of trenches is defined via a second EBL step, and the exposed Si_3N_4 area is etched away using reactive-ion etching (RIE). After RIE, the substrate is immersed in buffered hydrofluoric acid (49% concentration) for 15 seconds to etch the exposed SiO_2. Because the wet chemical etching is isotropic and selective with respect to Si_3N_4 and SiO_2, a stencil structure with a Si_3N_4 overhang is formed. The overhang is indicated in the schematic diagram in Figure 3b with a pair of black arrows, and the SEM image in Figure 3c clearly shows a Si_3N_4 overhang of about 500 nm width. The low internal stress of the Si_3N_4 layer permits the overhang to stand without collapsing into the trench. After this step, however, strong agitation, such as sonication, should be avoided in order to prevent any damage to the Si_3N_4 overhang (some damaged overhangs are shown in Supporting Information, Figure S3). The overhang is necessary for the electrical isolation of the metal NW deposited on the suspended DNA wire.

Even with the Si_3N_4 overhang, the electrical isolation may be compromised if a DNA wire suspended on the Si_3N_4 across a trench is broken and touches the bottom. To ensure electrical isolation of the NW in such a situation, several Au stripes are added via another step of EBL, thermal evaporation (Cr/Au, 5/50 nm), and gentle liftoff. A second hydrofluoric acid etching is then performed, which results in an overhang under the Au stripes that lay inside the trench, as depicted in the bottom panel of Figure 3b. This overhang ensures there is no additional electrical conducting path from any broken DNA

https://dx.doi.org/10.1021/acs.nanolett.0c03166
Nano Lett. 2020, 20, 8135−8140

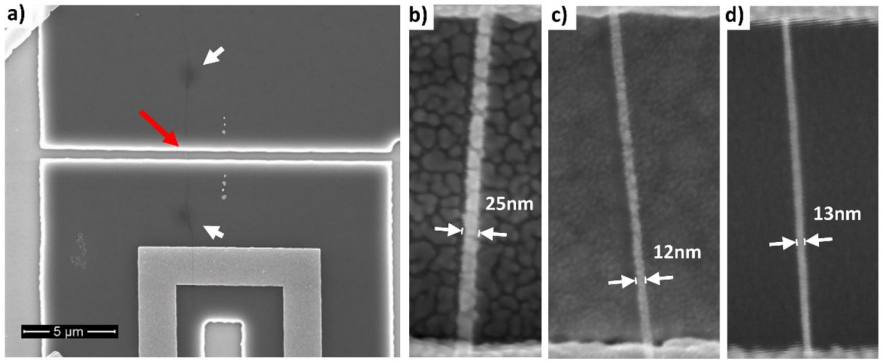

Figure 4. DNA wires before and after metal coating. (a) An SEM image of a DNA wire over and across a trench. The red arrow indicates where a DNA wire is located, and the shorter white arrows indicate where some of the micropillars contacted the substrate and left dark spots. To avoid damaging the insulating DNA wire, no close-up SEM imaging was performed before metal coating. (b) A DNA wire with Ge/Ag (5/32 nm) deposited at room temperature. (c) A DNA wire with Ge/Au (3/6 nm) deposited at room temperature. For both (b,c), the SEM imaging was performed at room temperature after *in situ* electrical measurements at room temperature. (d) A DNA wire with Sb/Pb (1.5/1.9 nm) deposited at cryogenic temperatures (<10 K). The SEM imaging was performed at room temperature after *in situ* electrical measurements at 4.2 K.

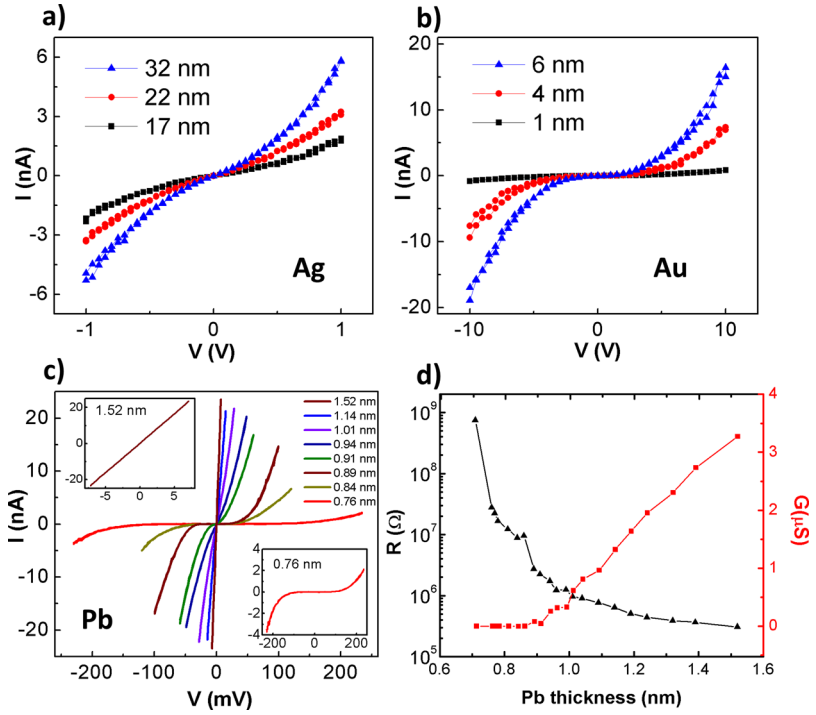

Figure 5. *In situ* transport measurements. (a) *I*−*V* curves of the same Ag NW at Ag thicknesses of 17, 22, and 32 nm. (b) *I*−*V* curves of the same Au NW at Au thicknesses of 1, 4, and 6 nm. In both cases, the *I*−*V* curves were measured *in situ* at different thicknesses at room temperature in the deposition system. The SEM images of the Ag and Au NWs after the final *I*−*V* measurements are shown in Figure 4b,c, respectively. (c) *I*−*V* curves of the same Pb NW at a series of different Pb thicknesses from 0.76 to 1.52 nm. The insets show the close-up *I*−*V* curves for the two extreme Pb thicknesses. A transition from nonlinear tunneling to linear Ohmic transport in this small thickness range is evident. (d) Zero-bias conductance (red squares) and high-bias differential resistance (black triangles) for the Pb NW in a range of Pb thicknesses. At 0.9 nm, the conductance begins to increase linearly with thickness, indicating the formation of a uniform Pb NW.

wire (after the metal coating). More details of the structure and fabrication of the Au stripes and associated overhang are described in Supporting Information, Section 3. Figure 3d shows an optical micrograph of a device ready for the transfer of the DNA wires. The horizontal thin red line is the trench that will be crossed by the DNA wires, and the wider vertical red lines are trenches for isolating different regions in the device. The bottom half of the device has four isolated areas; each can accommodate a DNA wire so that four metal NWs could be obtained simultaneously and each measured independently.

Using the DNA wire templates, we fabricated metal NWs out of three different materials (silver, gold, and lead). The contrasting morphologies of the resulting NWs from two different growth methods are shown in the SEM micrographs in Figure 4b−d. The first NWs (Ag and Au) were grown at room temperature in a thermal evaporation system. A Ge layer was first deposited to "wet" the DNA wire, and then Ag or Au was incrementally deposited, and a metal NW of varying thicknesses (cross-section) was obtained on the same DNA wire. After each deposition, quasi four-terminal *I*−*V* measurements were carried out *in situ* in the same vacuum system

https://dx.doi.org/10.1021/acs.nanolett.0c03166
Nano Lett. 2020, 20, 8135−8140

without any air exposure, thus enabling a systematic and reliable examination of the evolution of the electrical conductivity of the NW. Although a Ge buffer layer was used to promote uniform growth of Ag or Au, the resulting NWs still exhibit obvious granular morphologies, as shown in Figure 4b,c (see Supporting Information, Sections 5 and 6 for more details). As a result, the electrical transport was dominated by intergrain tunneling, as evidenced by the $I-V$ curves for a Ag and Au NW at different thicknesses shown in Figure 5a,b, respectively. Both sets of $I-V$ show significant nonlinearity at relatively large thicknesses, the Ag NW at up to 32 nm and the Au NW at 6 nm. This is consistent with the SEM images, which show substantially larger grains in the Ag NW than the Au NW. It is worth noting that the vastly different thickness dependencies of the $I-V$ curves for Ag and Au suggest that the contact of the metal deposited on the DNA wire with the Au electrodes has minimal contribution to the measured $I-V$ curves.

To minimize granularity and realize metal NWs of homogeneous morphology, we employed a method of low-temperature quench-condensation in our customized apparatus equipped with a cryogenic evaporator and *in situ* low-temperature electrical measurement capabilities. The DNA templates were loaded into the system, which was sealed and evacuated and then immersed in liquid helium. Once reaching base temperature, the system was naturally under ultrahigh vacuum. Under these conditions, the metal was deposited, and the electrical measurements were performed *in situ*. For this experiment, we used Sb as a buffer layer and Pb to form metal NWs. This scheme and material combination have been proven to produce uniform films down to monolayer thicknesses.[21−25] Here, with the template held at <10 K, an Sb layer of about 1.5 nm was first deposited. Subsequently, Pb was incrementally deposited to vary the thickness (cross-section) of the Pb NW. After each deposition, quasi-four-terminal $I-V$ measurements were carried out at the base temperature of 4.2 K. Figure 5c shows the evolution of the $I-V$ curves for one such NW at varying Pb thicknesses. The bottom and top insets show the $I-V$ curves for the thinnest and thickest NWs, respectively. The effective thickness of the films was measured *in situ* with a quartz crystal monitor located close to the substrate. Since the entire experiment of metal deposition and electrical measurements was conducted in ultrahigh vacuum and at low temperatures on one and the same NW, the effects of surface oxidation, structural annealing, and sample-to-sample variation are eliminated.

With increasing Pb thickness, it is evident that the $I-V$ curve evolves from a highly nonlinear insulating behavior to a linear Ohmic type. The nonlinear $I-V$ curves are characterized by a flat (high resistance) region suggestive of the Coulomb blockade.[26] The thickness range in which Coulomb blockade behavior in $I-V$ is present coincides with that of zero conductance region in Figure 5d, up to a thickness of 0.9 nm for this specific sample. Below this thickness, structural continuity and diffusive electrical conduction are probably not yet established in the NW. Beyond this thickness, the zero-bias conductance begins to increase linearly with thickness. Figure 5d also shows a semilogarithmic plot of the differential resistance at high bias voltage (black triangles) as a function of thickness, which similarly shows a transition from tunneling to linear transport. The results provided compelling evidence that a uniform, electrically continuous Pb NW was realized at a thickness of 0.9 nm and a width of 13 nm.

In summary, we have demonstrated the efficacy of using DNA NWs as templates to produce electrically continuous metal NWs of extremely small cross section. Using the same templates, two types of ultrathin metal NWs of contrasting morphologies were produced by room-temperature deposition and cryogenic-temperature quench-condensation. We demonstrated a high degree of predictability and control in the location, separation, and orientation of the NWs on a prepatterned substrate. With this procedure, we are able to reproducibly fabricate metal NWs with widths close to 10 nm. Electrical ($I-V$) measurements were performed *in situ* on both types of metal NWs upon incremental metal deposition, thereby providing a clear picture of the establishment and evolution of electrical continuity in these NWs. In particular, the method of low-temperature quench-condensation is shown to produce metallic NWs with cross sections as small as 12 nm^2. There is still room to further decrease the diameter of the stretched DNA wires by using smaller pillar diameters or lowering the DNA solution concentration.[19] Our results have shown the promise of this type of molecular templates as a viable platform for studying quantum transport in the true 1D limit, such as in 1D superconductors and associated devices, including Josephson junctions and SQUIDs.

■ ASSOCIATED CONTENT

Supporting Information

The Supporting Information is available free of charge at https://pubs.acs.org/doi/10.1021/acs.nanolett.0c03166.

Experimental methods, examples of damaged trenches, more details about the Au stripes for electrical isolation, removal of DNA utilizing an electron beam, more examples of NWs formed via quenched condensation, and NWs formed at room temperature (PDF)

■ AUTHOR INFORMATION

Corresponding Author

Peng Xiong − *Department of Physics, Florida State University, Tallahassee, Florida 32306, United States;* orcid.org/0000-0003-1746-1404; Email: pxiong@fsu.edu

Authors

Jorge L. Barreda − *Department of Physics, Florida State University, Tallahassee, Florida 32306, United States;* orcid.org/0000-0001-9816-9389

Longqian Hu − *Department of Physics, Florida State University, Tallahassee, Florida 32306, United States*

Liuqi Yu − *Department of Physics, Florida State University, Tallahassee, Florida 32306, United States*

Jacob Hudis − *Department of Physics, Florida State University, Tallahassee, Florida 32306, United States*

Timothy D. Keiper − *Department of Physics, Florida State University, Tallahassee, Florida 32306, United States*

Junfei Xia − *Department of Chemical and Biomedical Engineering, Florida A&M University−Florida State University College of Engineering, Florida State University, Tallahassee, Florida 32310, United States*

Zhibin Wang − *Department of Chemical and Biomedical Engineering, Florida A&M University−Florida State University College of Engineering, Florida State University, Tallahassee, Florida 32310, United States*

Jingjiao Guan − *Department of Chemical and Biomedical Engineering, Florida A&M University−Florida State University*

https://dx.doi.org/10.1021/acs.nanolett.0c03166
Nano Lett. 2020, 20, 8135−8140

College of Engineering, Florida State University, Tallahassee, Florida 32310, United States

Complete contact information is available at: https://pubs.acs.org/10.1021/acs.nanolett.0c03166

Author Contributions

J.L.B., T.D.K., and P.X. prepared the manuscript with contributions from all authors; J.G. and P.X. conceived the study; J.L.B., L.Y., J.X., Z.W., and J.G. characterized the DNA stretching and transferring; J.L.B. designed and fabricated the three-layer substrates; J.L.B. and T.D.K. performed the room-temperature experiments; J.L.B., L.H., and J.H. performed the cryogenic experiments; J.L.B. and P.X. analyzed and interpreted the results. All authors have given approval to the final version of the manuscript.

Notes

The authors declare no competing financial interest.

■ ACKNOWLEDGMENTS

The authors thank Stephan von Molnár, Hanwei Gao, and David Van Winkle for their valuable comments and discussions and Eric Lochner, Kurt Koetz, Joe Ryan, Robert Smith, and Ian Winger for technical assistance. This work was supported by NSF Grants DMR-1905843 and DMR-1828090.

■ ABBREVIATIONS

NW	nanowire
PDMS	polydimethylsiloxane
EBL	electron-beam lithography
RIE	reactive ion etching

■ REFERENCES

(1) Amato, M.; Rurali, R. Surface physics of semiconducting nanowires. *Prog. Surf. Sci.* **2016**, *91* (1), 1−28.
(2) Sun, Y.; et al. Compositional and structural engineering of inorganic nanowires toward advanced properties and applications. *InfoMat* **2019**, *1* (4), 496−524.
(3) Lieber, C. M.; Wang, Z. L. Functional nanowires. *MRS Bull.* **2007**, *32* (2), 99−108.
(4) Weber, W. M.; et al. Reconfigurable nanowire electronics - A review. *Solid-State Electron.* **2014**, *102*, 12−24.
(5) Quan, L. N.; Rand, B. P.; Friend, R. H.; Mhaisalkar, S. G.; Lee, T.-W.; Sargent, E. H. Nanowires for Photonics. *Chem. Rev.* **2019**, *119*, 7444.
(6) Noor, M. O.; Krull, U. J. Silicon nanowires as field-effect transducers for biosensor development: A review. *Anal. Chim. Acta* **2014**, *825*, 1−25.
(7) Yogeswaran, U.; Chen, S. M. A review on the electrochemical sensors and biosensors composed of nanowires as sensing material. *Sensors* **2008**, *8* (1), 290−313.
(8) Batra, A. K.; et al. Micro- and Nano-Structured Metal Oxides Based Chemical Sensors: An Overview. *J. Nanosci. Nanotechnol.* **2014**, *14* (2), 2065−2085.
(9) Larsen, T. W.; et al. Semiconductor-nanowire-based superconducting qubit. *Phys. Rev. Lett.* **2015**, *115* (12), 127001.
(10) Mourik, V.; et al. Signatures of Majorana fermions in hybrid superconductor-semiconductor nanowire devices. *Science* **2012**, *336* (6084), 1003−1007.
(11) Deng, M.; et al. Majorana bound state in a coupled quantum-dot hybrid-nanowire system. *Science* **2016**, *354* (6319), 1557−1562.
(12) Zhang, H.; Liu, D. E.; Wimmer, M.; Kouwenhoven, L. P. Next steps of quantum transport in Majorana nanowire devices. *Nat. Commun.* **2019**, *10* (1), 1−7.
(13) Hobbs, R. G.; Petkov, N.; Holmes, J. D. Semiconductor nanowire fabrication by bottom-up and top-down paradigms. *Chem. Mater.* **2012**, *24* (11), 1975−1991.
(14) Lu, W.; Lieber, C. M. Nanoelectronics from the bottom up, in Nanoscience And Technology: A Collection of Reviews from Nature Journals. *World Scientific* **2009**, 137−146.
(15) Bollinger, A. T.; Rogachev, A.; Remeika, M.; Bezryadin, A. Effect of morphology on the superconductor-insulator transition in one-dimensional nanowires. *Phys. Rev. B: Condens. Matter Mater. Phys.* **2004**, *69* (18), 180503 DOI: 10.1103/PhysRevB.69.180503.
(16) Bezryadin, A.; Lau, C. N.; Tinkham, M. Quantum suppression of superconductivity in ultrathin nanowires. *Nature* **2000**, *404* (6781), 971−974.
(17) Hopkins, D. S.; et al. Quantum interference device made by DNA templating of superconducting nanowires. *Science* **2005**, *308* (5729), 1762−1765.
(18) Hopkins, D. S.; Pekker, D.; Wei, T.-C.; Goldbart, P. M.; Bezryadin, A. Local superfluid densities probed via current-induced superconducting phase gradients. *Phys. Rev. B: Condens. Matter Mater. Phys.* **2007**, *76* (22), 220506 DOI: 10.1103/PhysRevB.76.220506.
(19) Guan, J. J.; et al. Simultaneous fabrication of hybrid arrays of nanowires and micro/nanoparticles by dewetting on micropillars. *Soft Matter* **2007**, *3* (11), 1369−1371.
(20) Guan, J. J.; Yu, B.; Lee, L. J. Forming highly ordered arrays of functionalized polymer nanowires by dewetting on micropillars. *Adv. Mater.* **2007**, *19* (9), 1212−1217.
(21) Valles, J. M.; Dynes, R. C.; Garno, J. P. Electron-tunneling determination of the order-parameter amplitude at the superconductor-insulator transition in 2d. *Phys. Rev. Lett.* **1992**, *69* (24), 3567−3570.
(22) Xiong, P.; Herzog, A. V.; Dynes, R. C. Superconductivity in ultrathin quench-condensed Pb/Sb and Pb/Ge multilayers. *Phys. Rev. B: Condens. Matter Mater. Phys.* **1995**, *52* (5), 3795−3801.
(23) Xiong, P.; Herzog, A.; Dynes, R. Negative magnetoresistance in homogeneous amorphous superconducting Pb wires. *Phys. Rev. Lett.* **1997**, *78* (5), 927.
(24) Parker, J.; et al. Superconducting quantum phase transitions tuned by magnetic impurity and magnetic field in ultrathin a-Pb films. *EPL (Europhysics Letters)* **2006**, *75* (6), 950.
(25) Gardner, H. J.; Kumar, A.; Yu, L.; Xiong, P.; Warusawithana, M. P.; Wang, L.; Vafek, O.; Schlom, D. G. Enhancement of superconductivity by a parallel magnetic field in two-dimensional superconductors. *Nat. Phys.* **2011**, *7* (11), 895−900.
(26) Tapio, K.; et al. Toward single electron nanoelectronics using self-assembled DNA structure. *Nano Lett.* **2016**, *16* (11), 6780−6786.